

# Quantum spin Hall effect and spin-charge separation in kagomé lattice

Zhigang Wang<sup>1</sup> and Ping Zhang<sup>1,2,\*</sup>

<sup>1</sup>*LCP, Institute of Applied Physics and Computational Mathematics,  
P.O. Box 8009, Beijing 100088, People's Republic of China*

<sup>2</sup>*Center for Applied Physics and Technology, Peking University, Beijing 100871, People's Republic of China*  
(Dated: September 14, 2009)

A two-dimensional kagomé lattice has been theoretically investigated within a simple tight-binding model, which includes the nearest neighbor hopping term and the intrinsic spin-orbit interaction between the next nearest neighbors. By using the topological winding properties of the spin-edge states on the complex-energy Riemann surface, the spin Hall conductance is obtained to be quantized as  $-e/2\pi$  ( $e/2\pi$ ) in insulating phases. This result keeps consistent with the numerical linear-response calculation and the  $\mathbf{Z}_2$  topological invariance analysis. When the sample boundaries are connected in twist, by which two defects with  $\pi$  flux are introduced, we obtain the spin-charge separated solitons at  $1/3$  (or  $2/3$ ) filling.

PACS numbers: 73.43.-f, 71.10.Pm, 72.25.Hg

Over the last two decades the topological band insulators (TBIs) have been a subject of great interest in condensed matter field<sup>1,2</sup>. Different from the normal band insulators, the TBIs have a prominent characteristic, which is the necessary presence of gapless edge states on the sample boundary<sup>3,4</sup>. An early TBI model was proposed by Haldane<sup>5</sup>. Therein it was shown that the gapless edge states result in a remarkable feature of TBIs by showing a quantum Hall effect in absence of a macroscopic magnetic field. Besides the Haldane model, several other lattice models have been proposed to be the quantum Hall TBIs, which include the two-dimensional (2D) spin-chiral kagomé lattice<sup>6,7</sup> and the three-dimensional (3D) distorted fcc lattice<sup>8,9</sup>. All the quantum Hall TBIs rely on the breaking of time-reversal symmetry (TRS).

Recently, Kane and Mele generalized the spinless Haldane model to a spin one by adding an intrinsic spin-orbit interaction (SOI)<sup>10,11</sup>. The TRS is conserved in the Kane-Mele model and the gapless spin edge states in this model result in a quantum spin Hall effect. These TBIs like the Kane-Mele model keeping TRS are different from the quantum Hall TBIs, and we call them the quantum spin Hall TBIs. The quantum spin Hall TBIs have received considerable attention. One impressive example is that only one year later after its theoretical prediction to be a quantum spin Hall TBI in 2006<sup>12</sup>, it was proved in experiment that HgTe is an actual one<sup>13</sup>.

One special character of the quantum spin Hall TBIs was recently attributed to their spin-charge separated excitations<sup>14,15</sup> in the presence of a  $\pi$  flux. This attribution is motivated by the recent advance in studying 2D fractionalized quasiparticles<sup>16,17</sup>, and is a straightforward result when, like what Kane and Mele<sup>10</sup> have dealt with Haldane's TBI, considering spins of the 2D edge soliton. The separate spinon, holon, and chargeon obey Bose statistics and the experimental measurement of these soliton excitations would provide an undoubted verification of the  $\mathbf{Z}_2$  topological properties of the quantum spin Hall TBIs. At present, besides the necessity for further studies to gain more insights into the nature

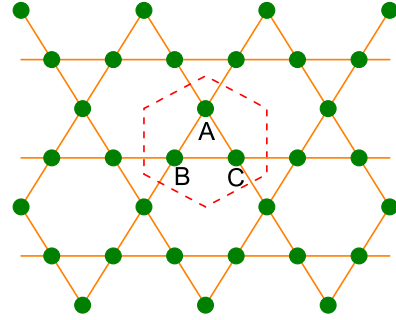


FIG. 1: (Color online). Schematic picture of the 2D kagomé lattice. The dashed lines represent the Wigner-Seitz unit cell, which contains three independent sites (A, B, C).

of spin-charge separation and its connection to the other topological phenomena, obviously, it is also important to identify and study various model systems that exhibit the phenomenon of spin-charge separation. Motivated by this observation, as well as by the recent attention on the layered metal oxides as possible candidates for the quantum spin Hall TBI<sup>18</sup>, in this paper, we study the quantum spin Hall effect and construct spin-charge separated edge solitons in 2D kagomé lattice. Different from the previously studied kagomé TBI<sup>6,7,19</sup> wherein the presence of ferromagnetic spin chirality breaks TRS, here TRS persists and the quantum spin Hall effect occurs due to the intrinsic SOI. By using the bulk linear-response theory, as well as the topological winding numbers of the spin-edge states on the complex-energy Riemann surface, we obtain the spin Hall conductance (SHC)  $\sigma_{xy}^s$ . The quantized value of  $\sigma_{xy}^s$  is  $-e/2\pi$  ( $e/2\pi$ ) at  $1/3$  ( $2/3$ ) filling. Then, we construct spin-charge separated edge solitons by introducing  $\pi$  fluxes with a method similar to that in Ref.<sup>16</sup>. The quantum statistics of these solitons is also discussed.

Consider the tight-binding model for independent electrons on the 2D kagomé lattice (Fig. 1). The spin-

independent part of the Hamiltonian is given by

$$\mathcal{H}_0 = t \sum_{\langle ij \rangle \sigma} c_{i\sigma}^\dagger c_{j\sigma}, \quad (1)$$

where  $t_{ij}=t$  is the hopping amplitude between the nearest-neighbor link  $\langle ij \rangle$  and  $c_{i\sigma}^\dagger$  ( $c_{i\sigma}$ ) is the creation (annihilation) operator of an electron with spin  $\sigma$  (up or down) on lattice site  $i$ . For simplicity, we choose  $t=-1$  as the energy unit and the distance  $a$  between the nearest sites as the length unit throughout this paper.

The Hamiltonian (1) can be diagonalized in the momentum space as

$$\mathcal{H}_0 = \sum_{\mathbf{k}} \psi_{\mathbf{k}\sigma}^\dagger H_0(\mathbf{k}) \psi_{\mathbf{k}\sigma}, \quad (2)$$

where the electron field operator  $\psi_{\mathbf{k}\sigma} = (c_{A\mathbf{k}\sigma}, c_{B\mathbf{k}\sigma}, c_{C\mathbf{k}\sigma})^T$  includes the three lattice sites ( $A, B, C$ ) in the Wigner-Seitz unit cell shown in Fig. 1.  $H_0(\mathbf{k})$  is a  $3 \times 3$  spinless matrix given by

$$H_0(\mathbf{k}) = -t \begin{pmatrix} 0 & 2 \cos(\mathbf{k} \cdot \mathbf{a}_1) & 2 \cos(\mathbf{k} \cdot \mathbf{a}_3) \\ 2 \cos(\mathbf{k} \cdot \mathbf{a}_1) & 0 & 2 \cos(\mathbf{k} \cdot \mathbf{a}_2) \\ 2 \cos(\mathbf{k} \cdot \mathbf{a}_3) & 2 \cos(\mathbf{k} \cdot \mathbf{a}_2) & 0 \end{pmatrix}, \quad (3)$$

where  $\mathbf{a}_1 = (-1/2, -\sqrt{3}/2)$ ,  $\mathbf{a}_2 = (1, 0)$ , and  $\mathbf{a}_3 = (-1/2, \sqrt{3}/2)$  represent the displacements in a unit cell from A to B site, from B to C site, and from C to A site, respectively. In this notation, the first Brillouin zone (BZ) is a hexagon with the corners of  $\mathbf{K} = \pm(2\pi/3)\mathbf{a}_1, \pm(2\pi/3)\mathbf{a}_2, \pm(2\pi/3)\mathbf{a}_3$ .

The energy spectrum for spinless Hamiltonian  $H_0(\mathbf{k})$  is characterized by one dispersionless flat band ( $\epsilon_{1\mathbf{k}}^{(0)}=2$ ), which reflects the fact that the 2D kagomé lattice is a line graph of the honeycomb structure<sup>21</sup>, and two dispersive bands,  $\epsilon_{2(3)\mathbf{k}}^{(0)} = -1 \mp \sqrt{4b_{\mathbf{k}} - 3}$  with  $b_{\mathbf{k}} = \sum_{i=1}^3 \cos^2(\mathbf{k} \cdot \mathbf{a}_i)$ . These two dispersive bands touch at the corners ( $\mathbf{K}$ -points) of the BZ and exhibit Dirac-type energy spectra,  $\epsilon_{2(3)\mathbf{k}}^{(0)} = (-1 \mp \sqrt{3}|\mathbf{k} - \mathbf{K}|)$ , which implies a “particle-hole” symmetry with respect to the Fermi energy  $\epsilon_F = -1$ . The corresponding eigenstates of  $H_0(\mathbf{k})$  are given by

$$|u_{n\mathbf{k}}^{(0)}\rangle = G_{n\mathbf{k}}(q_{1\mathbf{k}}, q_{2\mathbf{k}}, q_{3\mathbf{k}})^T, \quad (4)$$

where the expressions of the components  $q_{i\mathbf{k}}$  and the normalized factor  $G_n(\mathbf{k})$  for each band are given in Table I.

TABLE I: The expressions for the coefficients in Eq. (4) with  $x_i = \mathbf{k} \cdot \mathbf{a}_i$ .

$q_{1\mathbf{k}}$	$\frac{1}{2}[\epsilon_{n\mathbf{k}}^{(0)2} - 4 \cos^2 x_2]$
$q_{2\mathbf{k}}$	$\epsilon_{n\mathbf{k}}^{(0)} \cos x_1 + 2 \cos x_2 \cos x_3$
$q_{3\mathbf{k}}$	$\epsilon_{n\mathbf{k}}^{(0)} \cos x_3 + 2 \cos x_2 \cos x_1$
$G_{n\mathbf{k}}^{-2}$	$2b_{\mathbf{k}}\epsilon_{n\mathbf{k}}^{(0)2} + [4b_{\mathbf{k}} - 3\epsilon_{n\mathbf{k}}^{(0)2}] \cos^2 x_2 + 6(b_{\mathbf{k}} - 1)\epsilon_{n\mathbf{k}}^{(0)}$

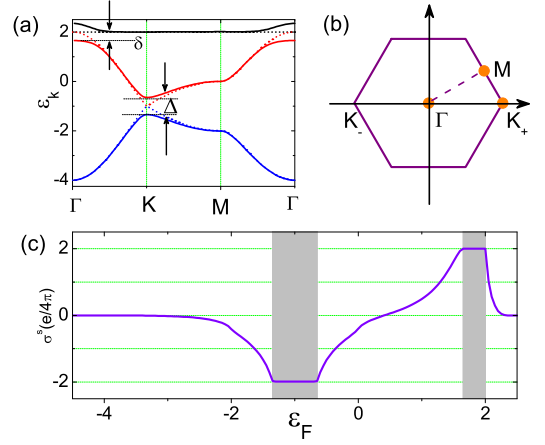


FIG. 2: (Color online). (a) Energy spectrum (solid curves) of the 2D kagomé lattice along the high-symmetry lines in the BZ with intrinsic spin-orbit couplings  $\lambda_{\text{SO}}=0.1t$ . There are two band gaps appearing with gap width  $\Delta$  and  $\delta$ . For comparison, we also draw the energy spectrum without intrinsic spin-orbit couplings (dotted lines). (b) The corresponding BZ of the 2D kagomé lattice. (c) The SHC  $\sigma_{xy}^s$  as a function of the Fermi energy  $\epsilon_F$ . The shaded areas correspond to the bulk gaps.

Then, we introduce the intrinsic SOI term, which, according to the symmetry of the kagomé lattice, takes the form<sup>10,22</sup>

$$\mathcal{H}_{\text{SO}} = i \frac{2\lambda_{\text{SO}}}{\sqrt{3}} \sum_{\langle\langle ij \rangle\rangle \sigma_1 \sigma_2} (\mathbf{d}_{ij}^1 \times \mathbf{d}_{ij}^2) \cdot \mathbf{s}_{\sigma_1 \sigma_2} c_{i\sigma_1}^\dagger c_{j\sigma_2}. \quad (5)$$

Here  $\lambda_{\text{SO}}$  represents the SOI strength,  $\mathbf{s}$  is the vector of Pauli spin matrices,  $i$  and  $j$  are next-nearest neighbors, and  $\mathbf{d}_{ij}^1$  and  $\mathbf{d}_{ij}^2$  are the vectors along the two bonds that connect  $i$  to  $j$ . Taking the Fourier transform, we have

$$\mathcal{H}_{\text{SO}} = \sum_{\mathbf{k}\sigma} \psi_{\mathbf{k}\sigma}^\dagger H_{\text{SO}}(\mathbf{k}) \psi_{\mathbf{k}\sigma}$$

with

$$H_{\text{SO}}(\mathbf{k}) = \pm 2\lambda_{\text{SO}} \begin{pmatrix} 0 & i \cos(\mathbf{k} \cdot \mathbf{b}_1) & -i \cos(\mathbf{k} \cdot \mathbf{b}_3) \\ -i \cos(\mathbf{k} \cdot \mathbf{b}_1) & 0 & i \cos(\mathbf{k} \cdot \mathbf{b}_2) \\ i \cos(\mathbf{k} \cdot \mathbf{b}_3) & -i \cos(\mathbf{k} \cdot \mathbf{b}_2) & 0 \end{pmatrix}, \quad (6)$$

where  $\mathbf{b}_1 = \mathbf{a}_3 - \mathbf{a}_2$ ,  $\mathbf{b}_2 = \mathbf{a}_1 - \mathbf{a}_3$ ,  $\mathbf{b}_3 = \mathbf{a}_2 - \mathbf{a}_1$ , and the  $+$ ( $-$ ) sign refers to spin up (down) electrons.

Inclusion of the intrinsic SOI in the Hamiltonian makes the appearance of the eigenstates  $|u_{n\mathbf{k}}\rangle$  and eigenenergies  $\epsilon_{n\mathbf{k}}$  very tedious except for at some high-symmetry  $\mathbf{k}$  points. Instead of writing their explicit forms, here we show in Fig. 2(a) (solid curves) the numerically calculated energy spectrum for the total Hamiltonian  $\mathcal{H} = \mathcal{H}_0 + \mathcal{H}_{\text{SO}}$  along the high-symmetry lines ( $\Gamma \rightarrow \mathbf{K}$ ,  $\mathbf{K} \rightarrow \mathbf{M}$ , and  $\mathbf{M} \rightarrow \Gamma$ ) in the BZ. The SOI coefficient is chosen to be  $\lambda_{\text{SO}} = 0.1t$ . For comparison we also plot in Fig.

2(a) (dashed curves) the energy spectrum in the absence of SOI ( $\lambda_{\text{SO}}=0$ ). One can see that while the spin degeneracies is not lifted by the presence of the intrinsic SOI, nevertheless, the Dirac contacts of the lower and middle bands at the  $\mathbf{K}$  point are removed and there evolves a direct gap between these two bands. The amplitude of this gap turns out to be  $\Delta=4\sqrt{3}|\lambda_{\text{SO}}|$ . Similarly, the original contact at the  $\mathbf{\Gamma}$  point between the middle and upper (flat) bands is also lifted by the presence of SOI and a gap with amplitude  $\delta$  is opened. However, this gap is an indirect one, i.e., the middle-band maximum and upper-band minimum are not at the same  $k$ -point.

To see the behavior of the system in the insulating state, we have calculated the SHC using the following Kubo formula<sup>23</sup>

$$\sigma_{xy}^s = -e\hbar \sum_{n \neq n', \mathbf{k}} [f(\epsilon_{n\mathbf{k}}) - f(\epsilon_{n'\mathbf{k}})] \times \frac{\text{Im} \langle u_{n\mathbf{k}} | \frac{1}{2} \{ \hat{v}_x, \hat{s}_z \} | u_{n'\mathbf{k}} \rangle \langle u_{n'\mathbf{k}} | \hat{v}_y | u_{n\mathbf{k}} \rangle}{(\epsilon_{n\mathbf{k}} - \epsilon_{n'\mathbf{k}})^2 + \eta^2}, \quad (7)$$

where  $\hat{\mathbf{v}}(\mathbf{k}) = \partial H(\mathbf{k}) / \hbar \partial \mathbf{k}$  and  $H(\mathbf{k}) = H_0(\mathbf{k}) + H_{\text{SO}}(\mathbf{k})$ . The calculated result at zero temperature is shown in Fig. 2(c) by varying the Fermi energy  $\epsilon_F$  with the SOI coefficient  $\lambda_{\text{SO}}=0.1t$ . From Fig. 2(c), one can see that initially the SHC  $\sigma_{xy}^s$  decreases as the filling factors of the (spin-degenerate) lower band increases, arriving at the minimum value  $-(e/2\pi)$  at  $\epsilon_F = -1.35$  ( $= -1 - \Delta/2$ ), a value corresponding to the top of the lower band. Then, as the Fermi energy  $\epsilon_F$  continues to vary in the first gap region (shaded area wherein  $-1.35 \leq \epsilon_F \leq -0.65$ ), the SHC keeps this minimum value unchanged. As shown in the following, this quantized SHC can be understood by the  $\mathbf{Z}_2$ -valued topological invariant associated with this quantum spin Hall phase<sup>11</sup>. When the Fermi energy increases to touch the bottom of the middle band at  $\epsilon_F = -0.65$  ( $= -1 + \Delta/2$ ), then the SHC suddenly switches up and rapidly increases when the Fermi energy goes through the middle two bands. When  $\epsilon_F$  increases at the top of the middle two bands ( $\epsilon_F = 1.65$ ),  $\sigma_{xy}^s$  arrives at the maximum value  $e/2\pi$ . Then as the Fermi energy  $\epsilon_F$  continues to vary in the second gap region (shaded area  $1.65 \leq \epsilon_F \leq 2$ ), the SHC  $\sigma_{xy}^s$  keeps this maximum value unchanged. When the Fermi energy increases to touch the bottom of the upper band at  $\epsilon_F = 2$ , the SHC then suddenly switches down and rapidly decreases when the Fermi energy goes through the upper band. Finally the SHC  $\sigma_{xy}^s$  decreases to disappear when the three spin-degenerate bulk bands are all fully occupied.

Topologically, the quantum spin Hall insulating state at 1/3 or 2/3 filling can be seen by calculating a selective  $\mathbf{Z}_2$ -valued invariant  $\nu^{11}$ , which is related to the parity eigenvalues  $\xi_{2m}(\Gamma_i)$  of the  $2m$ -th occupied energy band at the four time-reversal-invariant momenta  $\Gamma_i$ <sup>24</sup>. Very recently, Guo and Franz<sup>22</sup> have numerically calculated the eigenstate of  $\mathcal{H}_{\Gamma_i}$  and they found that three  $\xi$ 's are positive and one is negative. Although which of the four  $\xi$ 's is negative depends on the choice of the inversion

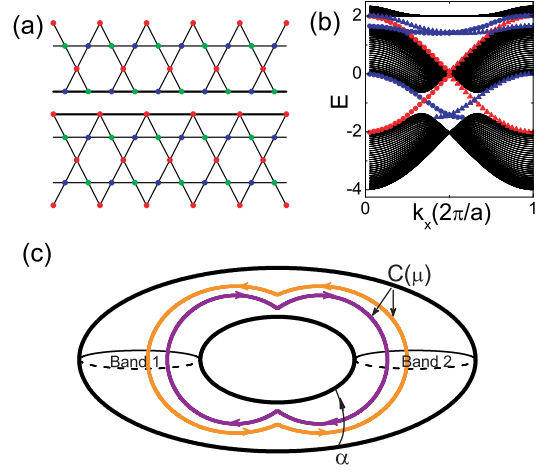


FIG. 3: (Color online). (a) Sketch of the 2D kagomé lattice strip with two edges along the  $y$  direction. The red, blue, and green dots are used to distinguish the independent sites A, B, and C, respectively. (b) Energy spectrum of the kagomé lattice strip ( $N_y=40$ ) with the Hamiltonian  $\mathcal{H}=\mathcal{H}_0 + \mathcal{H}_{\text{SO}}$ . The spin-orbit coupling strength is set as  $\lambda_{\text{SO}}=0.1t$ . The red and blue lines represent the edge states localized at the down and up edges of the system, respectively. And the circle and triangle label the up and down spins, respectively. (c) The Riemann surface of the Bloch function corresponding to 1/3 filling. The purple and orange curves correspond to spin-up and spin-down channels, respectively.

center, the product  $\Pi_i \xi(\Gamma_i) = (-1)^\nu$  is independent of this choice and determines the nontrivial  $\mathbf{Z}_2$  invariant  $\nu=1$ . That confirms the kagomé lattice system to be a quantum spin Hall TBI at 1/3 (or 2/3) filling.

On the other hand, the topological aspect of the quantized spin Hall phase can be distinguished by the difference between the winding numbers of the spin-up and spin-down edge states across the holes of the complex-energy Riemann surface,  $I_s = I_\uparrow - I_\downarrow$ <sup>20</sup>. The SHC is then given by  $\sigma_{xy}^s = I_s (e/4\pi)$ . Using this topological index  $I_s$  we have investigated the quantum spin Hall effect in the Kane-Mele graphene model<sup>20</sup>. For the present kagomé lattice model we can also study the quantum spin Hall effect in terms of this topological winding index. For this purpose, let us first numerically diagonalize the total Hamiltonian  $\mathcal{H}$  using the strip geometry. For convenience and without loss of generality, we suppose the system has two edges in the  $y$  direction while keeping infinite in the  $x$  direction [see Fig. 3(a)]. The number of sites A (or B, C) in the  $y$  direction is chosen to be  $N_y=40$ . The calculated energy spectrum is drawn in Fig. 3(b). From this figure one can clearly see that there are spin edge states occurring in each energy gap. These gapless edge states in the truncated kagomé lattice are topologically stable against random-potential perturbation, provided that the perturbation is small compared to the bulk gaps. We have numerically confirmed this fact. The Riemann surface of Bloch function is plotted

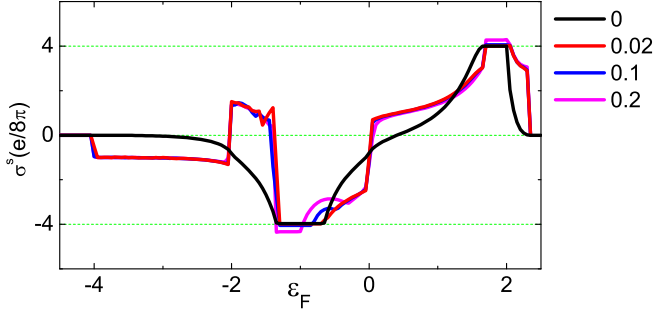


FIG. 4: (Color online). The SHC as a function of the Fermi energy  $\epsilon_F$  with different values of the Rashba coefficient. The black, red, blue, and pink lines correspond to  $\lambda_R=0, 0.02t, 0.1t$ , and  $0.2t$ , respectively. The intrinsic SOI strength is set as  $\lambda_{SO}=0.1t$ .

in Fig. 3(c) for  $1/3$  filling. According to Ref.<sup>20</sup>, the winding number of spin-up (spin-down) edge state in the lower gap is  $I_\uparrow=-1$  ( $I_\downarrow=1$ ), which gives  $I_s=-2$  at  $1/3$  filling. That means the SHC in this phase is quantized as  $\sigma_{xy}^s=-(e/2\pi)$ . The Riemann surface of Bloch function at  $2/3$  filling are the same as that at  $1/3$  filling, except that the directions of the curves corresponding to different spin channels are inverse. So the winding number of spin-up (spin-down) edge state in the upper gap is  $I_\uparrow=1$  ( $I_\downarrow=-1$ ), which gives  $I_s=2$ . The corresponding SHC at  $2/3$  filling is then quantized as  $\sigma_{xy}^s=e/2\pi$ . These conclusions are consistent with those calculated by using the Kubo formula (7) [see Fig. 2(c)]. Note that although the non-trivial  $\mathbf{Z}_2$  invariant  $\nu=1$  in the bulk analysis can confirm the quantum spin Hall TBI phase, it does not provide the information on the sign of the SHC. In contrast, our winding-number analysis can resolve this sign at different fillings (i.e.,  $\sigma_{xy}^s=\mp(e/2\pi)$  at  $1/3$  and  $2/3$  filling, respectively).

The topological properties of the system in the insulating state are stable even when the Rashba SOI is considered. To clearly see this fact, we numerically calculated the SHC  $\sigma_{xy}^s$  with the Kubo formula (7) when the total Hamiltonian includes the Rashba SOI<sup>25</sup>

$$\mathcal{H}_R = i \frac{\lambda_R}{\hbar} \sum_{\langle ij \rangle \sigma_1 \sigma_2} c_{i\sigma_1}^\dagger (\mathbf{s} \times \hat{\mathbf{d}}_{ij})_z c_{j\sigma_2}, \quad (8)$$

where  $\lambda_R$  is the Rashba coefficient and  $\hat{\mathbf{d}}_{ij}$  is a vector along the bond the electron traverses going from site  $j$  to  $i$ . The calculated SHC is drawn in Fig. 4 for different values of  $\lambda_R$ . Clearly, one can see that the amplitude of SHC in the insulating phase keeps  $e/2\pi$  unchanged when the Rashba SOI strength  $0 \leq \lambda_R/t < 0.1$ . When the Rashba SOI is sufficiently large (for example  $\lambda_R=0.2t$ ), the amplitude of SHC will depart little from the quantized value. However, the topology of this insulating state keeps unchanged, unless the bulk gaps disappear.

In the following let us consider the spin-charge separation in the 2D kagomé lattice. If we reconnect the

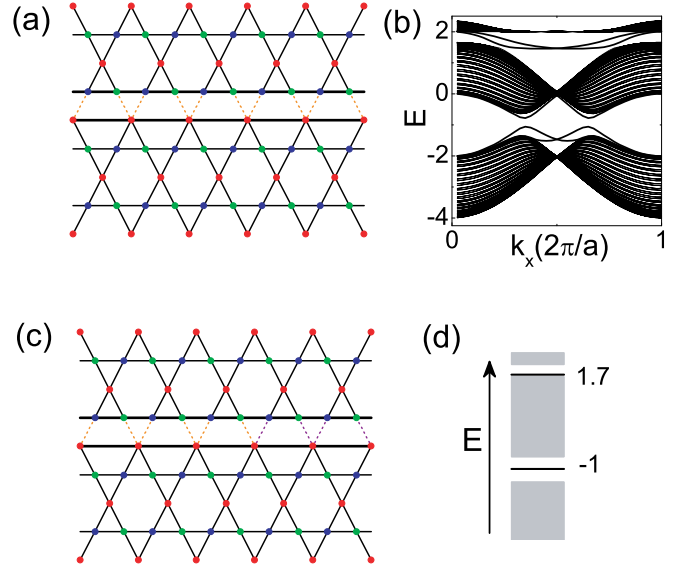


FIG. 5: (Color online). (a) Two edges of the 2D kagomé lattice are reconnected with weaker bonds (orange dotted lines) and its corresponding energy spectrum (b). (c) The restored bonds have a sign reversal along the right half bonds (violet dotted lines) and its corresponding energy spectrum (d). In these figures, the system size is set as  $N_y=40$  and the spin-orbit coupling  $\lambda_{SO}=0.1t$ . The bonds connected two edges are set as 0.25 times of other ones.

two edges of the kagomé lattice shown in Fig. 3(a) with weaker bonds, two small gaps then reappear in the edge spectrum [see Figs. 5(a) and (b)]. Topological excitations (edge solitons) are created by reversing the sign of the reconnected bonds along the right half row [see Fig. 5(c)]. In this manner two defects with  $\pi$  flux are introduced in the present kagomé lattice. As a result, four degenerate in-gap spin states localized around these two defects are formed in each bulk gap [see Figs. 5(d)]. The corresponding energies of these in-gap states are  $\epsilon=-t$  and  $1.7t$ , respectively. Note that in the square lattice version of the Kane-Mele model<sup>14</sup>, the in-gap modes are precisely at zero energy, while in the present kagomé lattice model the in-gap modes are no longer at zero energy.

At  $1/3$  or  $2/3$  filling, occupation (unoccupation) of these in-gap modes leads to an excess (deficit) of  $1/2$  fermion number per spin and per defect<sup>19</sup>. Four different types of solitons with the following quantum numbers are obtained when these in-gap modes are occupied by different ways: the chargeon  $f_{+(1/2)\uparrow,+(1/2)\downarrow}$  (charge  $-e$ ,  $S_z=0$ ); the holon  $f_{-(1/2)\uparrow,-(1/2)\downarrow}$  (charge  $e$ ,  $S_z=0$ ); the two spinons  $f_{+(1/2)\uparrow,-(1/2)\downarrow}$  (charge 0,  $S_z=\frac{\hbar}{2}$ ) and  $f_{-(1/2)\uparrow,+(1/2)\downarrow}$  (charge 0,  $S_z=-\frac{\hbar}{2}$ ). Here the subscript  $+$  ( $-$ ) represents that the in-gap mode is filled (empty) and  $\uparrow$  ( $\downarrow$ ) labels the spin mode. For example,  $f_{+(1/2)\uparrow,-(1/2)\downarrow}$  means that the up-spin mode is filled and the down-spin mode is empty. For further illustration, the charge-density distribution for the chargeon  $f_{+(1/2)\uparrow,+(1/2)\downarrow}$  is



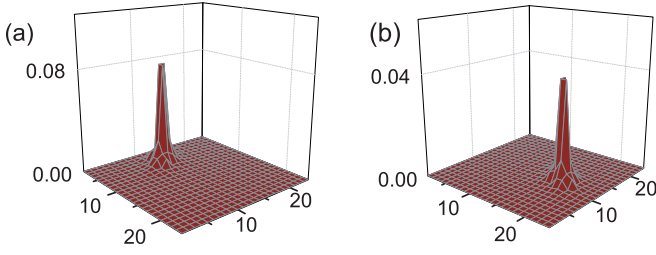


FIG. 6: (Color online). (a) The charge density of a chargeon state and (b) the spin density of a spinon on a  $24 \times 24$  lattice with periodic boundary condition. The chargeon at coordinate (6, 6) is  $f_{+(1/2)\uparrow,+(1/2)\downarrow}$ , it has charge  $-e$  and spin  $S_z=0$ . The spinon at coordinate (18, 18) is  $f_{+(1/2)\uparrow,-(1/2)\downarrow}$ , it has charge 0 and spin  $S_z=\hbar/2$ .

calculated and shown in Fig. 6(a), while the spin-density distribution for the spinon  $f_{+(1/2)\uparrow,-(1/2)\downarrow}$  is plotted in 6(b). Here, we use a  $24 \times 24$  lattice for calculation.

The quantum statistics of these spin-charge separated solitons can be readily seen by using anyon fusion argument<sup>14,26</sup>, which is based on the observation that the bound states of fractional excitation acquire non-trivial Berry phases on adiabatic exchange. Since the spin-up and spin-down bands in the present case decouple, so without loss of generality, let us consider a bound state of two identical spin-up solitons  $f_{(1/2)\uparrow}$  (or  $f_{-(1/2)\uparrow}$ ), which carries charge  $-e$  ( $e$ ) and flux  $2\pi \sim 0$  thus is a fermion. According to the anyon fusion rule, which states that the exchange phase  $\Theta$  of a particle formed by combining  $n$  identical anyons with exchange phase  $\theta$  is  $\Theta=n^2\theta$ , one easily obtain that the exchange phase between two identical solitons  $f_{(1/2)\uparrow}$  ( $f_{-(1/2)\uparrow}$ ) should be  $1/4$  that of fermions, i.e.,  $\theta(f_{(1/2)\uparrow}, f_{(1/2)\uparrow})$  (or  $\theta(f_{-(1/2)\uparrow}, f_{-(1/2)\uparrow}) = \pm\pi/4$ . Next let us consider a bound state of an  $f_{(1/2)\uparrow}$  and  $f_{-(1/2)\uparrow}$  soliton, which carries charge 0 and should be a boson. Then the

exchange phase between solitons  $f_{(1/2)\uparrow}$  and  $f_{-(1/2)\uparrow}$  is given by  $\theta(f_{(1/2)\uparrow}, f_{-(1/2)\uparrow}) = \mp\pi/4$ . Since the spin-down band is the Hermitian conjugate of the spin-up band one obtain  $\theta(f_{\alpha_1\downarrow}, f_{\alpha_2\downarrow}) = -\theta(f_{\alpha_1\uparrow}, f_{\alpha_2\uparrow})$ . Substituting these results into the formula calculating the exchange phase between spin-charge separated solitons  $\theta(f_{\alpha_1\uparrow\beta_1\downarrow}, f_{\alpha_2\uparrow\beta_2\downarrow}) = \theta(f_{\alpha_1\uparrow}, f_{\alpha_2\uparrow}) + \theta(f_{\beta_1\downarrow}, f_{\beta_2\downarrow})$ , one immediately concludes that the spinons, holons, and chargeon are all bosons. However, each spinon has nontrivial mutual exchange phase  $\pi$  with the chargeon and holon.

Before ending this paper, we would like to point out that the ways creating the spin-charge separated solitons in the kagomé lattice are not the only one. Recently Guo and Franz<sup>22</sup> suggested one possible realization of fractional charges  $\pm e/3$  or  $\pm 2e/3$  by trimerizing the kagomé lattice, like the 1D way proposed by Su and Schrieffer<sup>27</sup>. Based on this possible realization, if we introduce the intrinsic SOI in the considered Hamiltonian, then the spin-charge separated excitations are expected to appear with fractional charges  $\pm e/3$  and spins  $\pm \hbar/2$  and  $\pm \hbar/6$ . We leave this and the other interesting related problems to future study.

In summary, we have theoretically studied the quantum spin Hall effect and the spin-charge separation in the 2D kagomé lattice. By using the topological winding numbers of the spin-edge states on the complex-energy Riemann surface, we have obtained that the SHC is quantized as  $\pm(e/2\pi)$  when the system is in the insulating phase, which is consistent with the  $\mathbf{Z}_2$  topological invariant analysis and the numerical linear-response calculation. Furthermore, we have constructed the spin-charge separated solitons in kagomé lattice by connecting the system's boundaries in twist. The quantum statistics of these solitons has also been discussed.

This work was supported by NSFC under Grants No. 10604010, No. 10904005, and No. 60776063, and by the National Basic Research Program of China (973 Program) under Grant No. 2009CB929103.

\* Corresponding author. zhang\_ping@iapcm.ac.cn

<sup>1</sup> D. J. Thouless, M. Kohmoto, M. P. Nightingale, and M. den Nijs, Phys. Rev. Lett. **49**, 405 (1982).

<sup>2</sup> X.-G. Wen, *Quantum Field Theory of Many-Body Systems* (Oxford University Press, New York, 2004).

<sup>3</sup> B. I. Halperin, Phys. Rev. B **25**, 2185 (1982).

<sup>4</sup> Y. Hatsugai, Phys. Rev. Lett. **71**, 3697 (1993).

<sup>5</sup> F. D. M. Haldane, Phys. Rev. Lett. **61**, 2015 (1988).

<sup>6</sup> K. Ohgushi, S. Marakami, and N. Nagaosa, Phys. Rev. B **62**, R6065 (2000).

<sup>7</sup> Z. Wang and P. Zhang, Phys. Rev. B **76**, 064406 (2007); Phys. Rev. B **77**, 125119 (2008).

<sup>8</sup> R. Shindou and N. Nagaosa, Phys. Rev. Lett. **87**, 116801 (2001).

<sup>9</sup> Z. Wang, P. Zhang, and J. Shi, Phys. Rev. B **76**, 094406 (2007).

<sup>10</sup> C. L. Kane and E. J. Mele, Phys. Rev. Lett. **95**, 226801 (2005).

<sup>11</sup> C. L. Kane and E. J. Mele, Phys. Rev. Lett. **95**, 146802 (2005).

<sup>12</sup> B. A. Bernevig, T. L. Hughes, and S.-C. Zhang, Science **314**, 1757 (2006).

<sup>13</sup> M. Koenig, S. Wiedmann, Christoph Brüne, A. Roth, H. Buhmann, L. W. Molenkamp, X.-L. Qi, and S.-C. Zhang, Science **318**, 766 (2007).

<sup>14</sup> Y. Ran, A. Vishwanath, and D.-H. Lee, Phys. Rev. Lett. **101**, 086801 (2008).

<sup>15</sup> X.-L. Qi and S.-C. Zhang, Phys. Rev. Lett. **101**, 086802 (2008).

<sup>16</sup> D.-H. Lee, G.-M. Zhang, and T. Xiang, Phys. Rev. Lett. **99**, 196805 (2007).

<sup>17</sup> C.-Y. Hou, C. Chamon, and C. Mudry, Phys. Rev. Lett. **98**, 186809 (2007).

<sup>18</sup> A. Shitade, H. Katsura, J. Kuneš, X.-L. Qi, S.-C. Zhang, and N. Nagaosa, Phys. Rev. Lett. **102**, 256403 (2009).

<sup>19</sup> P. Zhang, Z. Wang, N. Hao, and W. Zhang (unpublished).

- <sup>20</sup> Z. Wang, N. Hao, and P. Zhang, arXiv: 0906.5118 (2009), to appear in Phys. Rev. B.
- <sup>21</sup> A. Mielke, J. Phys. A **24**, L73 (1991); **24**, 3311 (1991); **25**, 4335 (1992).
- <sup>22</sup> H.-M. Guo and M. Franz, arXiv: 0905.3385 (2009), to appear in Phys. Rev. B.
- <sup>23</sup> J. Sinova, D. Culcer, Q. Niu, N. A. Sinitsyn, T. Jungwirth, and A. H. MacDonald, Phys. Rev. Lett. **92**, 126603 (2004).
- <sup>24</sup> L. Fu and C. L. Kane, Phys. Rev. B **76**, 045302 (2007).
- <sup>25</sup> G. Liu, P. Zhang, Z. Wang, and S.-S. Li, Phys. Rev. B **79**, 035323 (2009).
- <sup>26</sup> C. Weaks, G. Rosenberg, B. Seradjeh and M. Franz, Nature Phys. **3**, 796 (2007).
- <sup>27</sup> W. P. Su and J. R. Schrieffer, Phys. Rev. Lett. **46**, 738 (1981).